Teknik Dergi, 2022 12677-12708, Paper 700

A Numerical Investigation on the Limitations of Design Equations for Steel Plate Shear Walls

Muhammed GÜRBÜZ[1]
İlker KAZAZ[2]

ABSTRACT

In previous studies various design issues on steel plate shear wall (SPSW) systems under lateral loading were investigated using analytical and experimental methods. However, these studies examined the interactive effect of only a few of design parameters, such as panel aspect ratio, column flexibility parameter, axial load ratio on the boundary frame columns, web plate thickness, stiffness of horizontal and vertical boundary elements and top anchor beam, etc., on the drift capacity and shear force distribution among frame and panel components of SPSWs at a time. This study investigates the effect of all of these parameters in the same framework. A parametric study is conducted on finite element models of 292 3-story SPSWs with rigid beam-to-column connections and designed for specified parameters. By evaluating failure forms from finite element analyses, the limiting (undesired) cases resulting from different combinations of specified geometric properties are identified. A column flexibility factor of 2.2 is proposed instead of the current limit value of 2.5 for satisfactory column performance, improved drift capacity and balanced strength distribution among frame and panel of SPSW. The value of 0.75 for the ratio of plate shear force to total shear force has emerged as a critical threshold value for the strength distribution among plate and frame components in order to fulfill capacity design principles. This study provides a comprehensive view of the behavior of SPWS for determining the most suitable combination of various parameters in the design of SPSW structures.

Keywords: Steel plate shear wall, finite element analysis, failure, column flexibility, axial load, inclination angle.

1. INTRODUCTION

Steel plate shear walls (SPSW) are structural components with high energy dissipation capacity, initial stiffness and ductility under lateral loads. Reduced seismic load due to

Note:
- This paper was received on October 6, 2021 and accepted for publication by the Editorial Board on April 8, 2022.
- Discussions on this paper will be accepted by November 30, 2022.
- https://doi.org/10.18400/tekderg.1005342

1 Erzurum Technical University, Civil Engineering Department, Erzurum, Turkey
muhammed.gurbuz@erzurum.edu.tr - https://orcid.org/0000-0001-6628-3363

2 Erzurum Technical University, Civil Engineering Department, Erzurum, Turkey
ilkerkazaz@erzurum.edu.tr - https://orcid.org/0000-0002-3885-1885

reduced dead weight and thickness of the walls are some of the advantages of the steel plate shear walls. These characteristics make them attractive for resisting seismic loading and dissipating seismic energy. A typical unstiffened steel plate shear wall consists of vertical and horizontal boundary elements (VBE and HBE) and an infill steel plate. There are different types of steel infill plates such as corrugated, perforated or stiffened. In some studies, sandwich composite panels used as infill plates to investigate the energy dissipation capacity change compared to unstiffened steel infill panels [1]. The desired behavior of properly designed unstiffened SPSWs under lateral loading can be represented by four phases. Figure 1 illustrates the anticipated behavior phases of a typical steel plate shear wall. Under a low level of loading, the entire structure should be elastic. After this phase, prior to global yielding, the central region of each panel is expected to yield, but the boundary elements remain to be elastic. At the global yielding except for the corner regions most parts of each panel yield and plastic hinges form at the beam ends. Finally, the entire panel yields and the plastic hinges form at the ends of all the beams and the first story column bases. The uniform yielding mechanism is fully developed in this stage. Except for the plastic hinges at the ends of boundary elements, in span regions must remain elastic; even the steel panel and the plastic hinges exhibit significant nonlinearity [2]. To assure this mechanism, codes and guidelines incorporate design equations and recommendations on the SPSW component's strength and stiffness.

The design equations and processes developed for SPSWs are based on well-established mechanical models. The shear strength of steel plate shear walls has been investigated by previous experimental research and accurately established by analytical research. Thorburn et al. [3] proposed an analytical model of yielding infill steel plate known as strip model, where the inclined tension field was represented by a series of pin-ended strips as shown in Figure 1. Timler and Kulak [4] verified the strip model presented by Thorburn et al. [3] by an experimental study on SPSWs. Tension field inclination angle (α) is developed using the principle of least work in these studies and is given as;

$$\tan^4 \alpha = \frac{1+\frac{t_w L_b}{2A_c}}{1+t_w h_s\left[\frac{1}{A_b}+\frac{h_s^{\,3}}{360 I_c L_b}\right]} \tag{1}$$

where t_w is the thickness of the infill plate, h_s is the story height, L_b is the bay width, I_c is the moment of inertia of the vertical boundary element, A_c is the cross-sectional area of the vertical boundary element, A_b is the cross-sectional area of the horizontal boundary element and α is the inclination angle of the strips.

The strip model enables the calculation of the shear capacity of SPSW. SPSW design requirements are given in AISC-341 [5], and practical low and high seismicity design processes are illustrated in AISC Design Guide 20 [6]. The story design shear strength given in AISC-341 originates from the strip model representing the collapse mechanism of a SPSW with simple connections, and it is derived as;

$$V_r = \frac{1}{2} F_y t_w L \sin 2\alpha \tag{2}$$

where F_y is the nominal yield stress of steel infill, L is the clear distance between VBE flanges (panel length) and other terms are as defined previously. For a frame with rigid beam-to-column connections, the overall shear capacity of a single-story frame V_r is defined as the sum of the shear capacities from moment frame and shear panel as presented in Eq.(3) [7].

$$V_r = \frac{1}{2} F_y t_w L \sin 2\alpha + \frac{4M_p}{h} \tag{3}$$

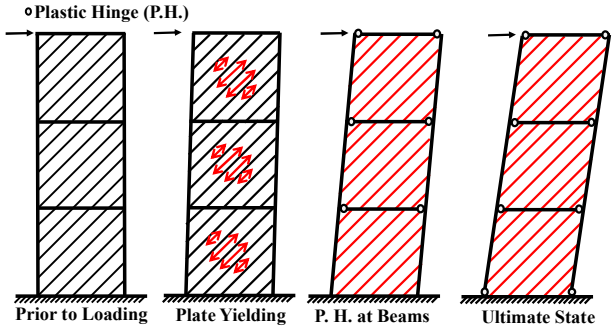

Figure 1- The anticipated sequence of failure mechanism of a multi-story steel plate shear wall with moment-resisting connections

In this equation, M_p is the smaller of plastic moment capacity of the beams or columns and h is the panel height. The shear force demand V_d under seismic loads are calculated using the soil class, maximum considered earthquake spectral response parameters, dead and live loads, etc. Taking $V_r \geq V_d$ in Eq. (2), the angle of tension field should be estimated, since the plate thickness and size of HBE and VBE required to be input in Eq. (1) are not initially known. As an initial value of inclination angle (α=45°) is assumed. Then, solving Eq. (2) for t_w, the thickness of the steel panel at a given story is determined. For these given equations to be valid, the size of boundary elements should be sufficiently stiff and strong for tension field development. Stiffness of bounding columns significantly affects the overall performance of steel plate shear wall (SPSW) systems under lateral loading conditions. Wagner's [8] analytical studies on diagonal tension fields provided the theoretical background on the flexibility coefficient of vertical boundary elements (ω_f). Wagner [3] derived the flange flexibility parameter by considering the elastic deformations of a cantilever plate girder under transverse loading. Kuhn et al. [9] simplified the flange flexibility parameter that is introduced by Wagner [8]. The simplified flexibility is used to specify the stiffness limits for the boundary frames. The given flexibility parameter is;

$$\omega_i \approx 0.7 h_{st} \left(\frac{t_w}{(I_u + I_0)L} \right)^{0.25} \tag{4}$$

where h_{st} stands for the spacing between the neighboring stiffeners, I_u is the moment of inertia of bottom flange (corresponding to the tension column of SPSW), I_o is the moment of inertia of top flange (corresponds to the compression column of the SPSW). Montgomery and Medhekar [10] proposed that the column flexibility parameter ω_i should not exceed 2.5 to form a relatively uniform tension field on steel plate shear walls. Considering both columns have the same moment of inertia and solving for I_c, Eq. (4) becomes:

$$I_c \geq \frac{0.00307 t_w h_s}{L_b} \tag{5}$$

Similarly, the horizontal boundary element element has a moment of inertia about the strong axis, I_b, not less than;

$$I_b \geq \frac{0.0031 L_b^4}{h_s} (t_{w,i+1} - t_{w,i}) \tag{6}$$

where $t_{w,i}$ is the infill panel thickness of the *i'th* story. As the steel panels have similar thicknesses at successive stories, Eq. (6) is ineffective to determine the beam size. In this study, a practical limit is adopted for I_c/I_b to determine I_b relative to column size. After designing the columns and beams, a refined estimation of tension field inclination angle is calculated using Eq. (1). Some iterations will help the design to be closer to have an optimal strength. Following the preliminary design, other calculations such as the boundary element compactness, shear strength, beam-to-column connection requirements, etc., should be checked.

Steel plate shear wall design equations briefly summarized above, are accommodated in various provisions and standards [5,11]. CAN\CSA 2009 [11] recommends that the infill plate of the SPSW should be designed to resist the entire load and neglects the contribution of the surrounding boundary frame as given in Eq. (2). AISC 2005 seismic provision [12] have the same approach on load resistance distribution over the infill plate and moment frame. The current building code, AISC 2016 [5], supersedes the previous approach and requires that the strength of the frame shall not be less than 25% of the total shear force, which finds a basis in the capacity design philosophy. The codes are ambiguous on whether the boundary frame contribution in the design of SPSW should be considered or not as given in Eq. (3). Purba and Bruneau [13] estimated the percentage of shear forces and suggested that the infill plates should be designed to resist the total story shear. Berman [14] analyzed the seismic behavior of a series of code-designed steel plate shear walls using nonlinear response history analysis with ground motions representing different hazard levels. The percentage of story shear resisted by the web plate relative to the boundary frame is between 60% and 80%, and it is relatively independent of panel aspect ratio, wall height or hazard level but is affected by the changes in plate thickness. Verma and Sahoo [15] studied the

contribution of boundary elements in resisting the lateral force considering their interaction with the web plates of SPSW systems. Results of nonlinear time-history analyses show that the percentage of lateral load resisted by infill plate depends on the aspect ratio of the infill and the number of stories. An expression was proposed to predict the lateral force contribution of the infill plate and the boundary frame of SPSWs based on stiffness. A series of code-designed steel plate shear walls (SPSWs) with different aspect ratios and number of stories were numerically analyzed to investigate the wall and frame contributions of SPSWs [16]. The design procedure that neglects the boundary frame-moment resisting action may result in quite different stiffness and ductility capacity on SPSWs with different aspect ratios under almost the same design lateral loads. The twenty-five percent frame resistance limit specified by the provision is somewhat arbitrary [17].

Another unclear issue in the preliminary design is the sizing of the horizontal boundary elements at the upper and lowermost levels. A lack of proper capacity design on the boundary elements may lead to the plastic hinges forming within the beam span or column height. These undesirable plastic mechanisms may induce significant inelastic deformations of the boundary elements and reduce the SPSW strength as it prevents the yielding of the corner region of the steel panels. Qin et al. [18] investigated the flexural behavior of anchor horizontal boundary element (top beam) in steel plate shear wall and found that the plastic flexural capacity of anchor HBE decreases from unity to the minimum as a result of an increase in shear force, axial force and vertical stresses. Dastfan and Driver [19] studied flexibility parameter limits for the top and bottom anchor beams and developed a new flexibility parameter (ω_L) for top and bottom anchor beams where the original assumptions do not apply. For the top beam, a limit of 2.5 is selected, and for the bottom panel an upper limit of 2 is proposed. A lower limit of $\omega_L \geq 0.84\omega_i$ is also introduced.

Yu et al. [20] tested a 1/3-scale, one-bay and two-story SPSW specimen under quasi-static cyclic loading and an axial load ratio of 0.3 ($0.3F_yA_g$) to investigate the behavior of steel plate shear walls with axially loaded vertical boundary elements. They conducted a parametric study of SPSW specimens with various width-to-height ratios of infill steel plates and axial load ratios of VBEs by the finite element analysis. They stated that without considering the effect of axial load, the VBE flexibility coefficient limit of 2.5 is applicable for the SPSWs with width-to-height ratio of 1.0 for the infill steel plate. However, with an increase of the infill steel plate's aspect ratio, the development of the tension field tends to be inadequate, while the shear capacity and stress uniformity of the infill steel plate decrease. As a result, the flexibility coefficient limit of 2.1 is recommended for the design of VBEs in SPSW structures. On the other hand, Curcovic et al. [21] stated that the current requirement for minimum column moment of inertia is conservative. Qu et al. [22] investigated the effect of column stiffness (flexibility) on drift concentration in steel plate shear walls. They stated that column stiffness should be a design parameter to ensure a reasonably uniform drift distribution and a more uniform infill plate yielding along the height of SPSW buildings. Qu and Bruneau [23] showed that the existing limit on ω_i is not correlated with satisfactory in-plane and out-of-plane VBE performance. Based on experimental data and analytical investigations, they examined whether the significant inward VBE inelastic deformation and out-of-plane buckling observed in some instances were due to excessive VBE flexibilities or due to other causes such as shear yielding at the ends of the VBEs. Sahoo et al. [24] investigated the effect of the type of connections between the web plates and the boundary elements and the boundary members' flexibility along with pinned beam-to-column

connections under lateral loading conditions using an experimental study on two-story SPSW specimens. Based on the analytical and experimental results, various design issues of SPSW systems are discussed.

The panel aspect ratio is one of the critical parameters that affect the shear distribution between the infill plates and VBEs. In AISC 05 [12], the ratio of panel width (L) to height (h) is limited to $0.8 \leq L/h \leq 2.5$. Aspect ratio and bay width of the steel plate shear walls were studied extensively by researchers. Gholipour and Alinia [25] studied the behavior of 4, 7, 10, 13, 16, and 19 story code-designed steel plate shear wall structures regarding panel aspect ratios of 0.83, 1.67, and 2.5, and it was concluded that selection of a suitable bay-width produces a considerable reduction on the size of VBE sections, especially in high-rise SPSWs. Li and Tsai [2] tested narrow SPSWs and stated that the SPSW exhibited ductile hysteretic behavior comparable to larger aspect ratios. Formisano et al. [26] conducted finite element analyses of slender steel shear panels regarding different values of the thickness by varying the aspect ratio of the plate for assessing the design formulas and the influence of the geometry on the structural behavior of shear plates.

This study is a comprehensive comparative study covering all aspects of SPSW preliminary design parameters and expounds on the correlation of the parameters with structural behavior. For that purpose, a numerical parametric study is devised to investigate the effect of a wide range of parameters such as plate thickness, aspect ratio, axial load and relative stiffness of boundary elements on the behavior of SPSW models using finite element analysis. In the numerical models, the top anchor beam is designed using different flexibility coefficients, and resultant behavior modes are reported. Both code-limited columns (flexibility parameter less than 2.5) and columns that violate requirements (column flexibility parameter above the limit 2.5) are considered. A wide range of aspect ratios are investigated, and the effect of aspect ratio on shear force distribution between plate and frame is quantified in terms of most influential parameters. The findings of this study give an insight on the effect of the relative shear strength of the infill plate with respect to total wall strength on the overall system behavior. Although the damage limits and failure development stages are studied well for the conventional shear walls [27], there is also need for detailed studies for SPSWs. This study investigates the failure sequences of SPSWs under monotonic loading in detail.

At the first stage, the finite element modeling procedure is verified using the experimentally measured response of shear wall specimens. In the parametric study, a total of 292 shear wall models combining various parameters are analyzed. The primary parameters affecting shear wall response are determined and adequacy of design equations are evaluated in emphasis to non-conforming cases.

2. FINITE ELEMENT MODEL VERIFICATION

Six different steel plate shear wall specimens from four different studies are selected for finite element model validation as displayed in Fig 2. Specific details of the specimens may be found elsewhere, so only necessary information is provided. A summary of the specimen properties that is used for validation is provided at Table 1.

Table 1- Properties of the specimens used for validation

Researcher	Specimen	No. of Stories	t_w (mm)	F_{yp} (MPa)	F_{yf} (MPa)	Column Section	Beam Section
Lubell et al. (2000)	SPSW2	1	1.5	320	380	S75x8	S75x8
Wang et al. (2015)	TM2	3	4[a]	288-418[b]	323-365[b]	250x200x8x12[a]	200x200x8x12[a]
Park et al. (2007)	WC4T	3	4	351-441[b]	351-441[b]	250x250x9x12	200x200x16x16
Park et al. (2007)	SC2T	3	2	351	351-441[b]	250x250x20x20	200x200x16x16
Park et al. (2007)	SC4T	3	4	351-441[b]	351-441[b]	250x250x20x20	200x200x16x16
Choi and Park (2008)	FSPW2	3	4	299	353-385[b]	150x150x22x22	150x100x12x20

t_w: infill plate thickness; F_{yp}: Plate material yield strength; F_{yf}: Frame material yield strength.
[a] Control story (2nd story)
[b] Tensile coupon test result range of the material (different thicknesses)

The first specimen SPSW2 is a 1/4 scale model of a steel-framed office building core tested by Lubell [28] as displayed in Fig 2(a). The steel plate web thickness of SPSW2 is 1.5 mm. The distance between two vertical boundary elements centerlines is 900 mm. The steel plate has a width-to-height aspect ratio of 1. The second model specimen TM2 is a three-story unstiffened steel plate shear wall with a 1/3 scale [29]. Different plate thicknesses are used in different stories; 6 mm for the bottom story plate and 4 mm for the top two-story plates. The frame TM2 is designed as a moment frame with welded connections.

The third model (WC4T) shown in Fig 2(c) is a 1/3 model of three-story steel plate shear wall [30]. The infill plate thickness of the WC4T specimen is 4 mm. Plate and boundary member materials are SM490 (Korean Standard) with a yield strength of 330 MPa. Two other specimens from the same study namely SC2T and SC4T are also modelled and used for validation study. WC4T specimen has a column section of H-250×250×9×12 (H- overall depth × flange width × web thickness × flange thickness). SC4T and SC6T specimens have relatively strong columns (H-250×250×20×20). Infill plate thickness (t_w) of SC4T and SC6T specimens are 4 mm and 6 mm respectively.

The last specimen used for validation is frame designated as FSPW2 from the study by Choi and Park [31]. The columns of the three-story model have a section of H-150×150×22×22. The beams at second and third stories are H-150×100×12×20 and the top beam is H-250×150×12×20. The infill plate thickness of the specimen is 4 mm made of SS400 (Korean Standard) steel grade.

Detailed three-dimensional models of the specimens are created in ANSYS APDL [32] software. SHELL 181 from the ANSYS element library is used to create steel web plate and boundary elements of the models. The element has four nodes with six degrees of freedom at each node: translations in the x, y, and z directions and rotations about the x, y, and z axes. SHELL 181 element is also suitable for large strain nonlinear applications. Material properties are specified to be compatible with the materials used in the experiments and defined separately for each component of the model. Rate-independent material model is selected because all the experimental models were tested under static loading conditions. The steel material stress-strain curves are established as bilinear elastoplastic with von Mises yield criterion. Kinematic hardening rule is adopted for the models.

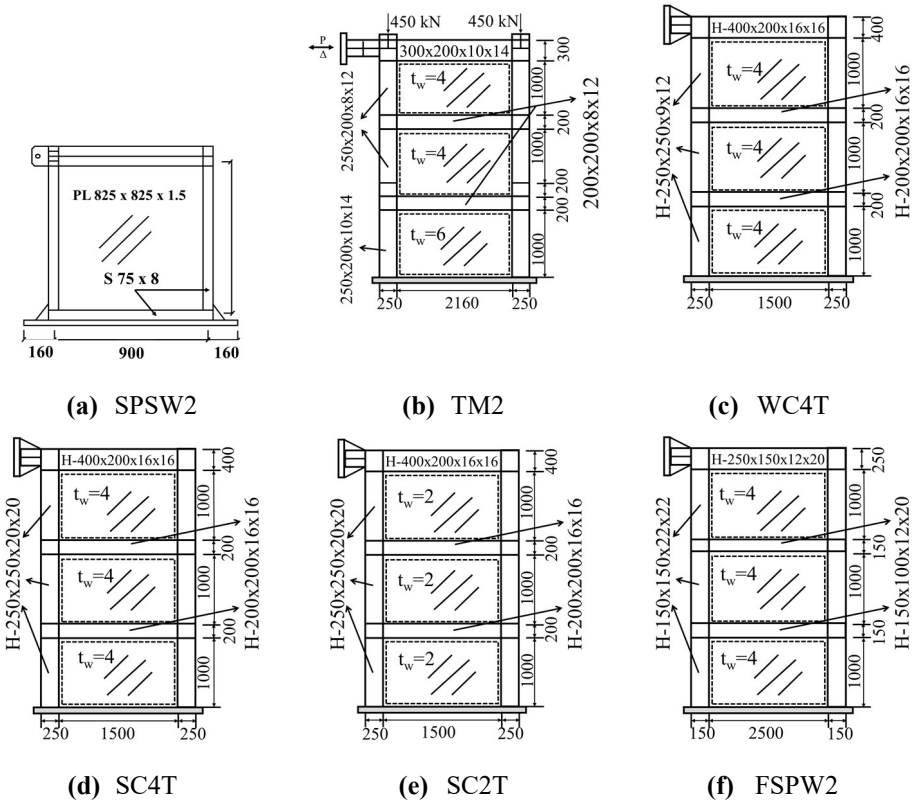

(a) SPSW2 **(b)** TM2 **(c)** WC4T

(d) SC4T **(e)** SC2T **(f)** FSPW2

Figure 2- Drawings of experimental models (a) SPSW2 [28] *(b) TM2* [29] *(c) WC4T* [30] *(d) SC4T* [30] *(e) SC2T* [30] *and (f) FSPW2* [31]

Steel plates have imperfections due to fabrication errors such as initial distortion due to welding or bolting processes, misalignment of boundary elements and infill plates, etc. Therefore, a small disturbance load initiating the out of plane displacement of infill plate is found to be adequate to produce the inherent wavy tension field pattern. A small force of 50–100 N is applied to avoid the possible counterbalancing force effect on the plate due to large values. It is verified that the location of the disturbance load on the infill plate has no effect on the analysis results and buckling shape. So, the disturbance load is applied at the middle of the plate simultaneously with vertical loads before the lateral loading in all analyses. Axial loads are applied at the column tops. When defining the boundary conditions, the models are fixed at the base. Nodes in regions corresponding to lateral support locations are restrained as specified in related studies.

All specimens were subjected to cyclic quasi-static loading in the experimental programs. In all the tests, steel plate shear walls exhibit good ductility [28–31] capacity and desirable energy dissipation. Figure 3 plots the monotonic and cyclic analyses results in comparison to experimentally measured responses. The agreement between global experimental results and numerical prediction can be considered to be satisfactory for all models. For three specimens

as the story displacements are available from experimental work, the inter-story drift ratios are compared in Figure 4. From the findings of this exercise, it is concluded that the numerical modeling tool and approach can be safely used in the parametric study.

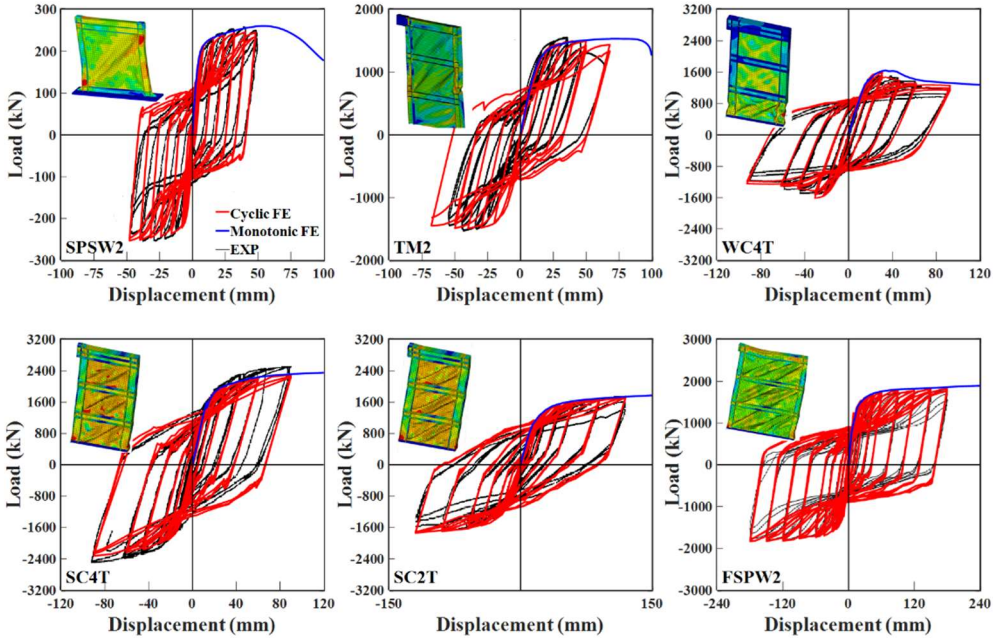

Figure 3 - Comparison of experimental and numerical load – top displacement curves

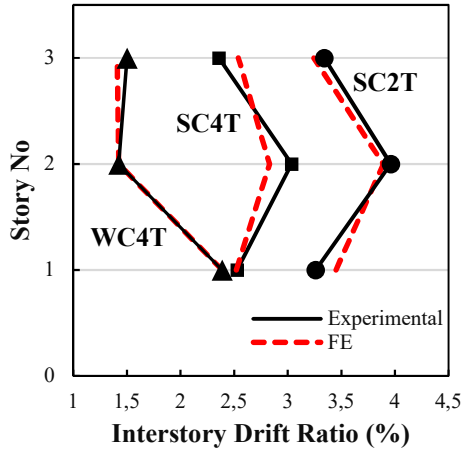

Figure 4 - Variations of maximum inter-story drift ratios

3. PARAMETRIC NUMERICAL STUDY ON SPSW SYSTEMS

3.1. Model Parameters

Plate thickness, panel aspect ratio, stiffness of boundary elements and axial load ratio on VBE are considered as the parameters to investigate the SPSW behavior. Both material and geometric nonlinearities are included in the models. A typical three-story SPSW model illustrating and summarizing the parameters of the study is presented in Figure 5(b). In order to increase the resistance of the top beam against the bending action of internal steel plate forces an additional beam is attached to the top beam, and the beams are assumed to be constrained (share the same nodes) along the adjoining beam flanges as shown in Figure 5(a). The horizontal load is applied at the top left nodes of the models as shown in Figure 5(b). Although the frame-wall interaction effects that may be influential on the behavior of SPSWs may be disregarded in this way, the relatively constant shear force at the base of building systems legitimize these models as much as experimental models. Beam to column intersections at all story levels are considered as the lateral support locations. Out-of-plane displacements of the nodes in intersection regions are restrained at all story levels. As explained in section 2, in all models a constant 50 N out-of-plane load is applied at the middle of the infill plate to account for the imperfections.

Capacity design procedures might result in highly conservative sections in some cases [14]. In order not to limit the parameters and define a wide range of models, the capacity design process has not been followed. Thus, a better observation of the parameter effects on SPSW behavior have been made. The steel panel height h_s is constant in all models as 3000 mm, and the selected panel lengths L are 2000, 3000, 4000, 5000, and 6000 mm. In this way, plate aspect ratios, which is defined as the ratio of panel length to height L/h, ranging from 0.67 to 2 are considered. Models with a low panel aspect ratio of 0.67 are analyzed as it was reported previously that narrow steel plate shear walls performed satisfactorily and exhibited ductile hysteric behavior, which can be compared to those with larger aspect ratios [2]. Plate thicknesses t_w are selected as 3, 4, 5, and 6 mm. Past research has focused on walls with a L/t_w ratio ranging from 300 to 800, although no limits are specified for that ratio as per AISC provisions [5]. The selected plate thickness and plate lengths cover a wide range of panel slenderness ($300<L/t_w<3000$).

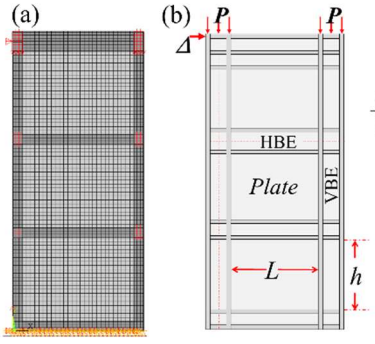

h (mm)	L (mm)	t_w (mm)	I_c/I_b	P/P_{cr}
3000	2000	2	1	0.1
	3000	3	2	0.2
	4000	4	3	0.3
	5000	5	4	
	6000	6	5	

Figure 5 - (a) A representative finite element model of SPSWs used in this study, (b) typical steel plate shear wall configuration

European rolled wide-flange sections are used to design HBEs (HE sections) and VBEs (HD sections). Structural steel grades of S235 (F_y=235 MPa, F_u=360 MPa) and S355 (F_y=355 MPa, F_u=510 MPa) are used for steel infill panel and the boundary elements, respectively. Vertical boundary elements are chosen according to the stiffness requirements as per the AISC seismic provisions. After determining h, L, and t_w, the required minimum value of column moment of inertia $I_{c,min}$ is calculated using Eq. (5). Then, different models are generated with I_c equal to 1, 2, 4, 6, 8, 10 times the required minimum value $I_{c,min}$. The sections (HD and HE) are selected according to their moment of inertia. In all cases, the section with the closest moment of inertia to the calculated I_c is selected without further consideration.

Additionally, models that do not meet the column flexibility requirements (Eqs. 4 and 5) are created to investigate the effects of non-conforming column flexibility on the overall behavior of the structure. The column flexibility factors (ω_1) of models models vaied from varied from 1.18 to 2.7. The models that have a column flexibility parameter greater than 2.7 are not considered as their poor performance has been recognized in previous studies [29]. According to the seismic design principle of SPSW, the boundary elements shall remain elastic under the forces of a fully yielded web plate. Only plastic hinges at the ends of the horizontal boundary elements are permitted at this stage. The moment of inertia of the HBE depends on the difference of web plate thicknesses at neighboring stories. Since the plate thicknesses at all stories are constant, the demand on the beam is insignificant, which makes Eq. (6) useless. So, the moment of inertia of the horizontal boundary elements is selected depending on the I_c/I_b ratio (I_c=moment of inertia of VBE, I_b=moment of inertia of HBE). The adopted column-to-beam moment of inertia ratios are in a range of $1 \leq I_c/I_b \leq 5$. After specifying the sections for columns and beams, the tension field inclination angle is calculated using Eq. (1). For investigating the effect of axial load on the shear capacity, VBEs are subjected to axial load levels of 0.1, 0.2, and 0.3 times the critical axial load P_{cr}, where P_{cr} is equal to the yield strength of the VBE material (F_y) times the cross-sectional area of the VBE (A_g). The combination of these parameters gives a total of 292 different three-story SPSW models. After the design process, the beam flange width to beam height ratio (b_f/h_b) and the beam flange width-to-thickness ratio ($b_f/2t_f$) also emerge as parameters which are considered in the parametric evaluation. The $b_f/2t_f$ ratio is used to determine whether the selected section is compact, non-compact, or slender with respect to limits specified in the standards. The lower the value of this parameter, the more compact the section is. With these two parameters, accurate observations could be made in cases where the I_c/I_b ratio was not sufficient to explain the beam behavior.

3.2. Structural Behavior under Monotonic Loading

As there is a large number of FE models for the analyses and considering the excessive solution time and the convergence difficulties in nonlinear cyclic loading analyses, all models are analyzed under monotonically increasing lateral load. Comparison of calculated load-deformation curves of experimental specimens under monotonic and cyclic loading indicates a larger drift capacity for the former than the latter for all experimental models as displayed in Figure 3. Traditionally, deformation limits of a subassembly should be derived using the experimentally obtained inelastic force–deformation cyclic response characteristics. Tests using monotonic loading are permitted to supplement the cyclic tests. However, the ultimate deformation need not be limited by that from the cyclic tests, where in-cycle rapid strength

loss did not occur during any cyclic test. In such cases, it is permitted to construct backbones from a combination of monotonic and cyclic data. The ultimate deformation of a cyclic test generally corresponds to the monotonic test capping displacement (at which the tangent stiffness becomes negative). The maximum displacement attained in the monotonic test is approximately 1.5 times that for the cyclic test. It is also known that the structural components (beam to column connections, infill plate, beams, and columns) may be exposed to more severe strength degradation under cyclic loading. So, it is occasionally argued that the cyclic loading protocol induced damage might be more severe than an actual seismic ground motion should do. Thus, there are cases where monotonic loading may produce more representative behavior of a subassembly. Monotonic loading adequately calculates the initial stiffness, maximum shear force and deformation characteristics within the eligible design drift ratio limits for all cases, which for this study is of interest.

Structural members and components are designed to exhibit a predetermined behavior under prescribed lateral load effect. So, the results of finite element analyses are evaluated on the basis of SPSW behavior. Buckling of infill steel plate is the first and inherent instability mode for all SPSW models. It should be useful to define the desired nonlinear behavior of an SPSW at this stage as a reference behavior type. The failure sequence of properly designed SPWS in reference to Figure 1 can be listed as;

- Buckling of steel infill plate and development of complete tension field action (yielding of the entire plate) at around 0.01 rad story drift ratio,
- Onset of yielding at the beam ends,
- Onset of yielding at column base,
- Plastic hinging at each end of the beam,
- Plastic hinging at the column base.

Obviously under such a variety of parametric combinations it should not be expected that all models will fail in this hierarchal order even if the design is performed under given limitations. It is observed that combination of parameters over a certain critical range leads to some unpredictable and undesirable failure patterns. By identifying these failure modes, the design parameters that cause such system behavior can be easily detected. For that purpose, the observed failure modes of SPSWs in the finite element analyses are identified as follows:

- Plastic hinge formation at horizontal boundary element,
- Plastic hinge formation at vertical boundary element,
- An apparent inward deformation on the vertical boundary element and in-plane shear yielding failure at the top end of VBE,
- Top anchor beam ends have in-plane plastic deformation under the axially acting column shear forces and steel panel-induced load,
- An in-span out-of-plane buckling at the top anchor beam,
- Yielding of beam-to-column junctions,
- Bending of VBE,
- VBE yielding along the height,
- In-span out-of-plane buckling along the height of the column.

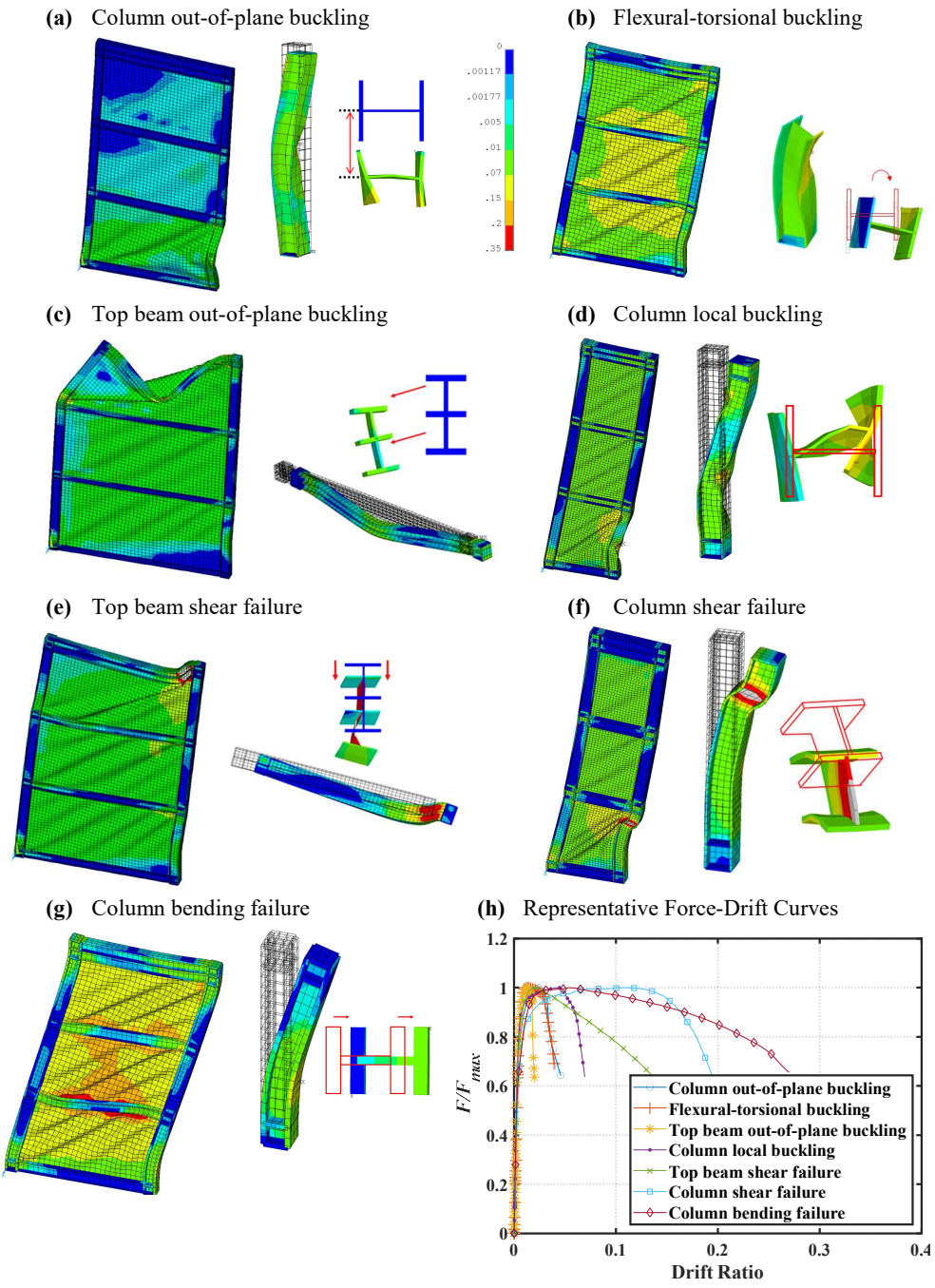

Figure 6 - Von-Mises strain plot of observed failure modes on models and specific column and beam members and representative lateral force-drift ratio curves of each mode

In the light of these failure definitions, seven main failure groups under monotonic loading are identified according to the dominant failure patterns as summarized in Figure 6. The von Mises strain plots for all failure modes are illustrated using the same contour levels given in Figure 6(a). It should be noted that some models may be classified under two or more groups as they exhibit more than one apparent failure modes. After grouping of models with similar failure patterns, the effects of design parameters on the SPSW behavior is investigated. The failure modes given in Figure 6(a-g) are studied in detail and the design parameters in relation to the specific failure pattern are determined by evaluating their effect on the load-deformation characteristics, i.e. shear force and lateral drift capacity. A representative lateral force-top drift ratio curve is selected from each group and they are plotted in Figure 6(h) for comparative and illustrative purposes.

The relationship between design parameters and the ratio of the shear force resisted by infill plate to total SPSW shear force (V_p/V_t) is investigated. The plate shear force is calculated using the forces from the nodes at the middle level of the first-story plate. The representative V_p/V_t value is adopted as the yield point on the load-deformation curve. The concept of equivalent plastic energy is used to determine the yield point.

Although some parameters reveal apparent trends with respect to drift capacity of models, such as increasing the axial load ratio P/P_{cr} on the boundary columns has a decreasing effect on the ultimate drift ratio, the plot of individual parameters displays a weak correlation with the ultimate drift ratio for the entire data set. So, the relation of design parameters with ultimate drift ratio is separately evaluated for each failure group as plotted in Figures 7 to 13. The ultimate drift ratio is defined as the point where the base story shear force drops 85% of the maximum value on the load-displacement curve. However, such high axial load cases where the force-displacement curve gradually decreases after peak force, the ultimate drift limit is accepted as the drift level which corresponds to 50% of the peak shear force. In the following individual failure modes illustrated in Figure 6 are examined in more detail.

3.2.1. Column out-of-Plane Buckling

As a general examination procedure, the correlation of SPSW design parameters with respect to ultimate drift ratio (first row) and ratio of plate shear force to total shear force V_p/V_t (second row) are plotted in Figure 7. This investigation procedure is also followed for all the remaining failure groups.

Main parameters affecting the column out-of-plane buckling are the column flexibility parameter ω_1 and the axial load ratio P/P_{cr}. Although buckling occurs with respect to the weak axis of VBE on this failure type, it is related to the ω_1, since the weak axis and strong axis moment of inertias are inter-related. The lowest ω_1 value of models with an out-of-plane displacement of columns is 2.2 as shown in Figure 7(a) and (g). The average axial load level of models in this group is 0.21 and this is one of the highest values among the groups. In this set of models, the average ratio of beam flange width to beam height b_f/h_b is 0.97 with a low standard deviation of 0.07. The width-to-thickness ratio of the beam flanges ($b_f/2t_f$) has a wide range and is not an indicative parameter for this group of models. The average drift ratio of the group is 0.039, which is the lowest average drift ratio among groups. Increasing the axial load and the plate aspect ratio reduces the drift ratio as shown in Figures 7(e)&(f). Both

parameters increase the axial demands on the columns and lead to early column failure as a result of column out-of-plane deformation as shown in Figure 6(a). Another parameter that contributes to the formation of this failure mode is the I_c/I_b ratio as displayed in Figure 7(h). For this failure mode most models have I_c/I_b =1.0 and the average I_c/I_b ratio is 1.58, which is the second lowest among groups. The use of relatively strong beams as indicated by I_c/I_b and b_f/h_b ratios increase the occurrence of column failure mechanism before the beams. The steel infill plate does not entirely yield in this type of failure mode. The observed failure sequence is as follows:

- Partial tension yielding at the steel infill plate,
- Yielding of beam-to-column junctions,
- Yielding starts at the compression column,
- In-span out-of-plane buckling occurs at the column.

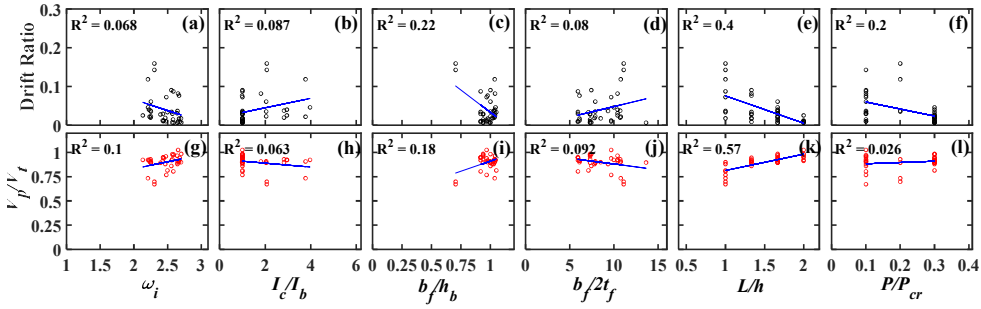

Figure 7 - Correlation of design parameters with drift and V_p/V_t ratios

In the design of steel plate shear walls, the boundary elements are expected to remain elastic until the entire plate yields. As the column failure starts prior to the entire plate yielding in this group, the frame contribution to the system shear capacity is minimal. The V_p/V_t ratio increases as the aspect ratio of the plate increases as displayed in Figure 7(k). Except for 4 of the 38 models in this group, all others have a V_p/V_t ratio greater than 0.8. These four models are characterized by the lowest column flexibility factor and aspect ratio of this failure group (L/h = 1.0). So, these four models have the largest deformation capacity of this set due to the stronger column and lower aspect ratio when compared to other models. It can be concluded that this type of failure is most likely to occur in SPSW designs with relatively weak columns ($\omega_i \geq 2.2$) and stiff and wide-flanged beams with $I_c/I_b \leq 1.58$ and $b_f/h_b \approx 0.97$, respectively. High axial load level significantly catalysis the failure, yet the failure mode may also commence under low axial load combined with critical values of these parameters.

3.2.2. Flexural Torsional Buckling of the Column

Flexural torsional buckling of a column usually takes place when sudden twists and bends occur in the member. In this failure group, the column is loaded eccentrically by the plate forces because of the deformed wavy shape of the steel infill. As illustrated in Figure 6(b),

eccentric stresses induced by the plate cause the column to twist and axial load facilities flexural buckling (average P/P_{cr} = 0.18). This group models have the second lowest average drift ratio level with an average value of 0.07. All models in this group have a plate aspect ratio of 1 and above as shown in Figure 8(k). The column flexibility factor is greater than 2.2 as in the first failure group as displayed in Figure 8(g). The average b_f/h_b ratio is 0.99 with a standard deviation of 0.04 as shown in Figure 8(i). The increasing axial load ratio and L/h ratio of the plate also correlates well with decreasing drift capacity in this group as displayed in Figures 8(e) and (f). In addition to increasing the compressive load on columns, high axial load also increases the P-delta effect and reduces the structural system's displacement capacity. The failure order of this failure type is:

- Tension yielding starts at steel infill panel while boundary elements remain elastic,
- Yielding develops at horizontal boundary element ends,
- Yielding initiates at vertical boundary element,
- Vertical boundary element cross-section rotates (twists) around the longitudinal axis of the member,
- An apparent inward deformation occurs at the vertical boundary element and VBE fails in the form of in-plane flexural buckling.

The V_p/V_t ratio is 0.73 and higher in all models. As the percentage of shear force resisted by the plate becomes dominant over the system strength, the drift ratio capacity of SPSW decreases. The plate shear force ratio has a strong relationship with the plate aspect ratio as shown in Figure 8(k). Although there is a correlation between drift and axial load level, V_p/V_t ratio remains insensitive to axial load level as displayed in Figures 8(f) and (l). The average column-to-beam stiffness ratio I_c/I_b and plate aspect ratio L/h of the first and second groups are 1.58 and 2.0 for the former and 1.5 and 1.22 for the latter, respectively. This indicates to relatively stiffer columns and narrower panel width for the second group than the first. Other parameters are similar in each group. It can be stated that narrow steel plate shear walls with ω_i above 2.2 and I_c/I_b <2.0 may not prevent the columns from being damaged before beams.

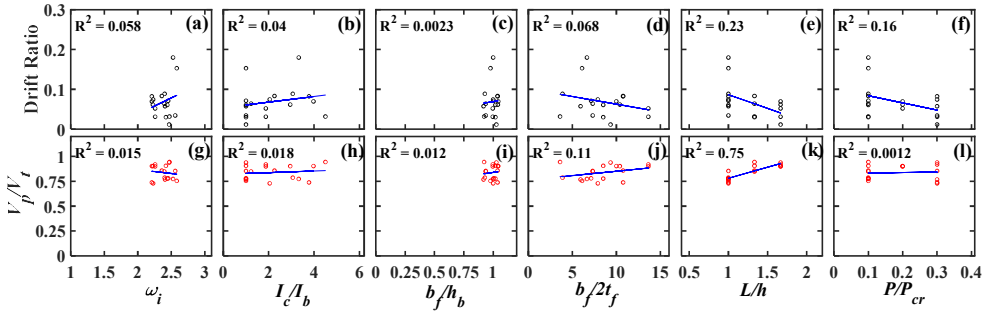

Figure 8 - Correlation of design parameters with drift and V_p/V_t ratios

3.2.3. Top Beam Out of Plane Buckling

Unlike the first two groups, the column flexibility factor covers a wide range of values for models of this group as shown in Figures 9(a) and (g). There is a significant decrease in the average axial load (P/P_{cr}= 0.14) when compared to first two groups. Figures 9(e) and (k) display that the models with the highest aspect ratios are clustered in this group. In all models, the proportion of plate width to height is 1.67 or 2.00. The average I_c/I_b ratio is 3.22, which is among the highest of all failure groups. The models in this failure group have more flexible horizontal boundary elements than vertical elements with a larger span. Using weak beams at inter-story is not influential to sudden failure. However, even double beams are used at the top of the frame, the stiffness is insufficient to resist out-of-plane buckling loads as illustrated in Figure 6(c). In this failure group, sudden strength loss without any softening behavior is observed on the load-displacement curve. This failure group has the highest average beam slenderness ratio. The slenderness ratio is calculated by dividing the story length (L_s) by the radius of gyration (r) of the cross Since buckling might occur about either of the axis, the radius of gyration about the weak axis is often becomes more important. As the beam length increases and the beam moment of inertia about weak axis decreases, the beams are more prone to buckling. Also, the low axial load prevents the columns from being damaged before the beams, which improves the systems lateral displacement capacity. The average ratio of the beam flange width to beam depth (b_f/h_b) is 0.77, which is lower than the first two failure groups and indicates to less stiff beam in the out-of-plane direction. For top beams, sections with a high b_f/h_b ratio and low I_c/I_b ratio reduce the occurrence probability of this type failure. The observed failure mechanism of this group is as follows:

- Partial/full yielding of the steel infill,
- Yielding of beam-to-column junctions,
- Yielding at column base and beam ends,
- Out of plane buckling of the top beam.

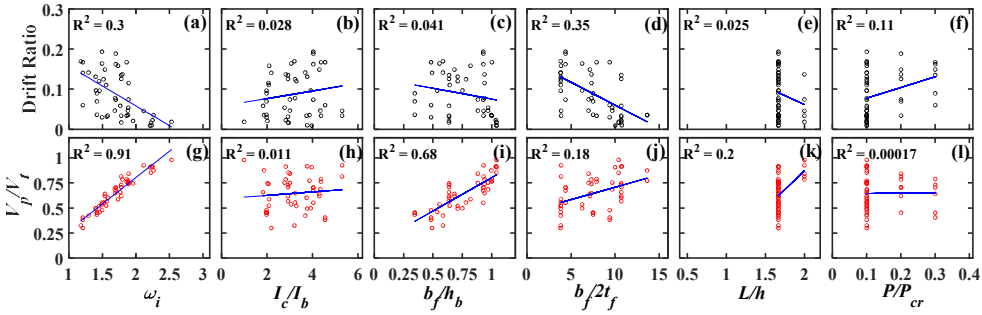

Figure 9 - Correlation of design parameters with drift and V_p/V_t ratios

The average drift ratio of this group is 0.09. There is an inverse correlation between column flexibility factor and drift ratio as displayed in Figure 9(a). The models in this failure group have stiffer columns than the models in the first two groups in terms of the moment of inertia. The average of column flexibility factors is 1.7. For V_p/V_t ratio, there is a noteworthy

correlation with the column flexibility factor (R-squared is 0.91) as plotted in Figure 9(g). The value of ω_f varies between 1.21 and 2.53. The results show that this failure mode may also develop in models with relatively weak columns represented with column flexibility factor greater than 2.2. But, note that these models are in the largest beam width to flange thickness ratio ($b_f/2t_f$>10) group. Even if the model has relatively weak columns (ω_f > 2.20), the top beam out-of-plane failure may occur with a combination of high L/h and high beam $b_f/2t_f$ ratios.

3.2.4. Column Local Buckling

Among the failure groups this particular failure mode is placed in the medium range in terms of average drift ratio. The average column flexibility factor ω_f is 2.14 with a lowest value of 1.7. Some models in this group can be classified under two or more groups as their deformed shape exhibit the failure properties of different modes at the same time. However, their common feature is that the failure initiates when local column flange buckling occurs and columns deform inwards as shown in Figure 6(d). In this group, the models with the highest aspect ratio (L/h=2.0) have the lowest drift ratio as displayed in Figure 10(e). Even so, if a model with a low aspect ratio (L/h =0.67) has a very high column flexibility factor, it may also fail at low drifts. In models with high aspect ratio, columns tend to deform nonlinearly before the entire infill panel yields. Models have a moderate axial load ratio (average is 0.18) in this group. In the models with the highest drift ratio, the local flange buckling usually occurs near the column base and leads to the formation of a plastic hinge. When the plastic hinges form in the column base and at the beam ends, this allows the structure to achieve high drift levels. When the plasticity develops within the column span, the drift ratio capacity decreases. In both scenarios, first the flange buckling initiates, and then instability develops. Two dominant failure sequences are:

- Yielding of the steel infill,
- Yielding of the beam-to-column junction,
- Yielding of beam ends,
- Yielding starts at column base,
- Plastic hinging at beam ends,
- Column local flange buckling near the base,
- Plastic hinging at the column base,

and,

- Partial yielding of the steel infill,
- Yielding of beam ends,
- Yielding starts at column base,
- Local flange buckling occurs in-span of the column,
- In-plane deformation of the column,
- Inward buckling – instability of the column.

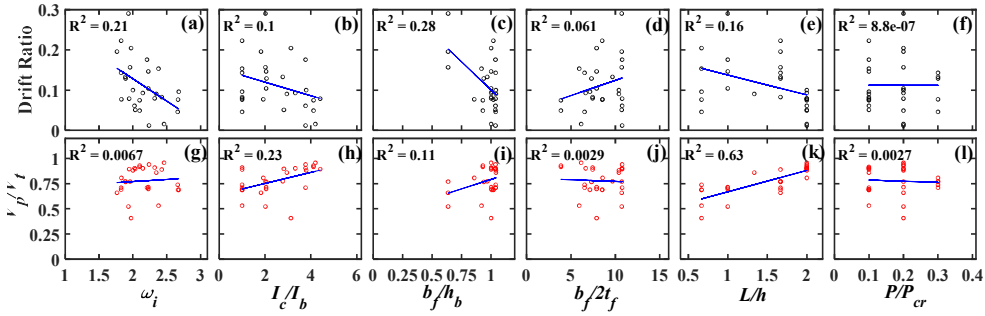

Figure 10 - Correlation of design parameters with drift and V_p/V_t ratios

Similar to other groups, the V_p/V_t ratio correlates with the plate aspect ratio as shown in Figure 10(k). Contribution of steel infill to the total base shear increases with the L/h ratio. This is because the columns fail before reaching their capacity. As seen in Figures 10(c) and (i), the b_f/h_b ratio of the models in this group is generally high. In models with high b_f/h_b ratio, while the beams have not been damaged yet, damage begins on the columns. In general, models with V_p/V_t ratio below 0.7 are models with a low plate aspect ratio and low column flexibility factor. Different combinations of these parameters can lead to different kinds of behavior.

3.2.5. Top Beam in-Plane Shear Failure

In this failure type, the top anchor beam end has inward deformation under steel panel-induced traction forces as displayed in Figure 6(e). The average ω_i e of the top beam shear failure group is 1.63, which is the lowest among all the failure groups. Strong columns enable models to reach high drift ratios. The average drift ratio of this group is 0.18, which is the second highest among groups. The average I_c/I_b ratio is the highest of all at 3.58. Some design parameters distinctly separate this group and the top beam out-of-plane deformation group discussed above. The plate aspect ratio L/h in the previous group is 1.7, which is the highest group average value, but in this group, this ratio is 1.2 and is one of the lowest. When the SPSW span length decreases, the upper beam is prone to shear failure with less possibility of out-of-plane deformation.

As given in Figure 11(a), column flexibility factor values of all models are less than 2.0 and the average b_f/h_b ratio is 0.68, which is the lowest of all groups. Only six models have an I_c/I_b ratio of less than 2.14. Although the value of beam stiffness is relatively large in these models, beam shear failure is triggered by low b_f/h_b ratio, which contributes to formation of local web or flange buckling at the upper beam's end under the unbalanced infill steel plate traction force. Models with a low b_f/h_b ratio do not always have low drift capacity. The low b_f/h_b ratio allows the models to have failure to form in beams rather than the columns, thus high drift ratios are achieved. The two main factors that permit this failure are low ω_i for columns and high I_c/I_b and low b_f/h_b ratios for beams. The failure sequence is as follows:

- Yielding of the steel infill,
- Yielding of beam ends,

- Yielding starts at column base,
- Plastic hinging at beam ends,
- Plastic hinging at the column base or in-plane column global buckling,
- Excessive inward deformation of the top beam end.

Most of the models have V_p/V_t ratios less than 0.7 as plotted in Figure 11(a). There is a good correlation between the column ω_i value and the V_p/V_t ratio as shown in Figure 11(g). A high ω_i value increases the V_p/V_t ratio in this group as in the other groups. Only five models, which are characterized with high ω_i, have V_p/V_t ratio above 0.7. It is also found that these five models have a b_f/h_b ratio of approximately 1 (see Figure 11(i)), which is quite above the average value and has high plate L/h ratio. Overall this group displays the strongest correlation between $b_f/2t_f$ and V_p/V_t ratios. Both parameters increase the V_p/V_t ratio as illustrated in Figures 11(j-k). In this group, which generally includes models with strong columns, an increase in the ratio of beam width to beam thickness $b_f/2t_f$ causes the upper beam to deform earlier. The drift ratios of these models are in the low to medium range.

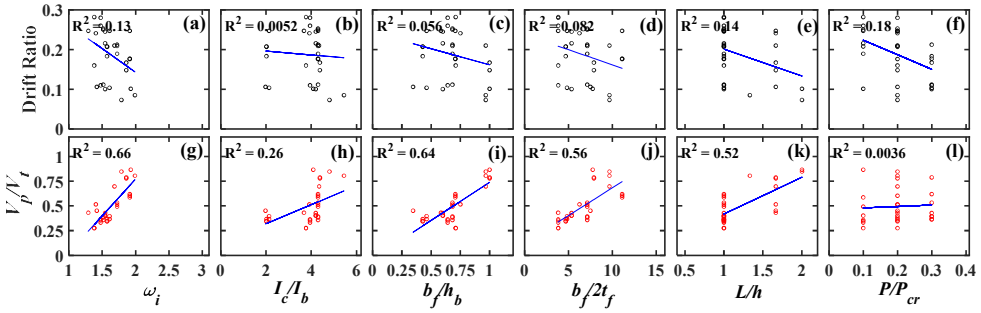

Figure 11 - Correlation of design parameters with drift and V_p/V_t ratios

3.2.6. Column Shear Failure

The models in this group have a shear failure at the compression column top end as illustrated in Figure 6(f). An apparent inward deformation occurs on the vertical boundary element and VBE fails in the form of in-plane shear yielding failure at the top. Only four models have column flexibility factor greater than 2.0 as seen in Figure 12(g). These four models have the lowest plate aspect ratio (L/h=0.67) and the minimum I_c/I_b value (1.0). High shear forces induced by stiff and short beams and inward forces from the steel infill plate lead to the formation of the column failure. This result indicates that when models with stiff columns ($\omega_i \leq 2.0$) are used together with beams of equal stiffness ($I_c/I_b \approx 1.0$), the beams are not damaged and failure occurs at the column top. As the minimum I_c/I_b ratio is 1.0, using sections with lower width to thickness ratio (low $b_f/2t_f$) makes the beams even more compact. For models with low ω_i as in this group, column shear yielding failure only occur using beam sections with the lowest I_c/I_b ratio and the lowest width to thickness ratio ($b_f/2t_f$) in the entire data set. This failure group has the lowest average I_c/I_b ratio (1.3) and the lowest average $b_f/2t_f$ ratio (3.87) among groups. In this group, which has the strongest beams of all groups in terms of stiffness and $b_f/2t_f$ ratio, the high shear force resulting from the opposing beam

and infill panel forces at the column top end ultimately leads to column shear failure. Although failure mechanism occurs on the columns, the average drift ratio of this group is 0.18, which is one of the highest. The failure sequence is as follows:

- Yielding of the steel infill,
- Yielding of beam ends,
- Yielding starts at column base and initiates through the height,
- Plastic inward deformation occurs at the column top level.

The V_p/V_t ratio of only two models in this group is above 0.75 as displayed in Figure 12. As seen in Figure 12(g), the V_p/V_t ratios plotted against the column flexibility factor ω_i indicates a moderate correlation with large dispersion. When the plate aspect ratio L/h is considered trend is similar to previous failure groups. As the aspect ratio of the plate increases, the V_p/V_t ratio also increases. The V_p/V_t ratio also increases with increasing beam $b_f/2t_f$ ratio. Models with the highest $b_f/2t_f$ ratio get the lowest values of ω_i in this failure group. The use of weaker columns and a higher $b_f/2t_f$ ratio on beams generally reduces the frame contribution to the shear strength of SPSW system.

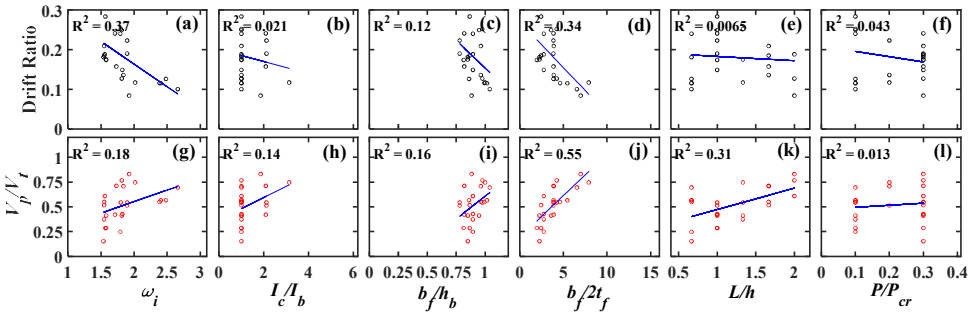

Figure 12 - Correlation of design parameters with drift and V_p/V_t ratios

3.2.7. Column Bending Failure

In this group, failure arises from the in-plane bending effect induced by infill plate forces along the column span. Local buckling does not form on the flanges and the web of the column, only flexural bending is observed along the length of the column as shown in Figure 6(g). The force-displacement curve of the SPSWs generally decrease gradually under bending and *P-Δ* effects, and no sudden strength drop is observed as illustrated in Figure 6(h). After the plastic hinge development at the beam ends, the columns deform under bending force and axial load. This group has the highest average drift ratio (≈0.21) as illustrated in Figure 13. The average axial load ratio is 0.22, which is one of the highest among groups. With a low column flexibility parameter, the SPSW system can have improved drift capacity even though the columns are exposed to high levels of axial load as in this failure type. The average value of the column flexibility factor is 1.67 as shown in Figures 13(a) and (g). Only 4% of the models in this group have ω_i values greater than 2.2. These models have low plate aspect ratio and low axial load. The trend between axial load

and drift ratio shows that the drift capacity decreases with increasing axial load as plotted in Figure 13(f). I_c/I_b ratio (≈2.57) of this group is higher than the column shear failure group and lower than the top beam shear failure group. Other parameters display similar tendencies with respect to drift and plate shear force ratio as with top beam shear failure and column shear failure groups. Based on these observations, it is concluded that the I_c/I_b ratio is an important parameter affecting the failure pattern of SPSWs. The failure sequence of this failure type is as follows:

- Yielding of the steel infill,
- Yielding of beam ends,
- Yielding starts at column base and initiates through the height,
- Plastic hinging at beam ends,
- Column bending.

Approximately 94% of the models have a V_p/V_t ratio below 0.75 as displayed in Figure 13(g). The average V_p/V_t ratio is 0.49, which is one of the lowest among the other groups. The V_p/V_t ratio has good correlation with $b_f/2t_f$ and increases with higher beam $b_f/2t_f$ ratio as shown in Figure 13(j). The V_p/V_t ratio also shows an increasing trend with increasing ω_i and L/h ratios of the plate, similar to other groups, as shown in Figure 13(g) and (k), respectively.

In general, this failure type has average parameter values comparable to the top beam shear failure group. Although the average values for ω_i and L/h are higher than the top beam shear failure group, the main reason for better drift performance is that the selected beams in this group are stiffer (average I_c/I_b=2.57) and have a lower $b_f/2t_f$ ratio, i.e. are strong beams.

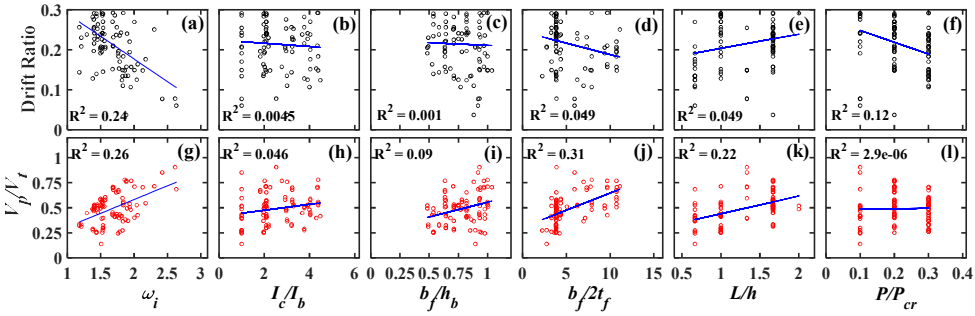

Figure 13 - Correlation of design parameters with drift and V_p/V_t ratios

3.3. Summary of Results

SPSW design parameters leading to different behavior types as identified above are summarized in Table 2 to gain better insight on the parametric relations that affect the failure pattern on SPSWs. In this way, effects of design parameters such as the axial load level and the stiffness of the horizontal boundary elements (in case of same thickness in adjacent stories), which are not addressed in the preliminary design code equations, can be evaluated comprehensively. Table 2 presents the average values of dependent and independent

variables calculated for seven groups. In Table 2, failure patterns are ordered with respect to decreasing column flexibility parameter ω_1. Due to strong correlation between ω_1 and V_p/V_t ratio, group average V_p/V_t values also became listed in ascending order. By this way, first three modes with the highest ω_1 become failure modes effected by column local flange instabilities. These modes are also characterized by medium panel aspect ratios (~1.5). These column instabilities are accompanied by low drift ratio and high V_p/V_t ratio. Low I_c/I_b ratios, high b_f/h_b and $b_f/2t_f$ ratios, i.e. relatively strong beams with respect to columns, are also peculiarities of these failure modes.

The last three failure modes in Table 2 are related to column and top beam in-plane deformations with high drift capacity and low V_p/V_t ratio. The main reasons of these behavior types are low column flexibility parameter ω_1 (stronger frames) and low L/h ratio (narrow SPSWs). Also, columns being stronger than beams characterized with high I_c/I_b ratio contributes to emergence of these failure modes. The fourth and fifth failure modes in Table 2 should be evaluated separately in our opinion. The top beam tends to experience outwards buckling when columns with moderate flexibility are utilized in high aspect ratio SPSWs. When the aspect ratio L/h of panel decrease, the instability of the top beam turns inwards. I_c/I_b ratio, another main ingredient of such behavior, is at the highest value for top beam shear buckling. Low b_f/h_b and $b_f/2t_f$ ratios increase the effect of mentioned parameters on top beam failures as seen in Table 2.

Table 2 - Average values of effective design parameters according to failure types.

No	Failure Type	Drift ratio	V_p/V_t	ω_1	L/h	P/P_{cr}	I_c/I_b	b_f/h_b	$b_f/2t_f$
1	Column out-of-plane buckling	0.04	0.89	2.46	1.50	0.21	1.58	0.97	8.49
2	Column flexural-torsional buckling	0.07	0.82	2.38	1.22	0.18	2.00	0.99	8.35
3	Column flange buckling	0.11	0.78	2.14	1.51	0.18	2.45	0.96	8.37
4	Top beam out-of-plane buckling	0.09	0.65	1.70	1.70	0.14	3.22	0.77	7.56
5	Top beam shear failure	0.18	0.49	1.63	1.20	0.20	3.80	0.68	6.62
6	Column shear failure	0.18	0.52	1.85	1.20	0.21	1.30	0.90	3.87
7	Column bending failure	0.21	0.49	1.67	1.30	0.22	2.57	0.78	5.47

When all groups are considered individually, a value of 2.2 emerges as a limiting value for the column flexibility factor for improved drift capacity and shear force distribution among the plate and frame parts of SPSW. In terms of drift ratio capacity, the ω_1 value of failure modes with the lowest drift capacity is above this limit. Models with a column flexibility factor greater than 2.2 may achieve high drift level, if certain criteria are met by other parameters. The number of these models has a very small percentage in the total data. The column flexibility factor above 2.2 leads to excessive column flexibility especially when high L/h and P/P_{cr} ratios are used. When the SPSW is designed for ω_1 values greater than 2.2, the wall is more likely to have a sudden strength drop on the load-deformation curve with the aggravating contribution of effects of other parameters to instability. The failure modes, such as partial yielding of the infill and sudden outward deformation failures of beams and columns, are more likely to occur in these models that do not meet the proper design considerations.

The use of high infill plate ratio L/h with high column flexibility factor results in failure modes with a relatively low drift capacity as discussed above. The failure modes with the highest drift capacity in Table 2 have the lowest L/h ratio. However, this should not indicate that wide SPSWs (with high L/h ratios) cannot be employed safely. When carefully combined with other parameters, it is observed that walls with high aspect ratios achieve high drift values. For example, in a model with the column flexibility factor ω_1 of 1.4 and the highest plate aspect ratio L/h=2.0, the column fails in global buckling by reaching a high level of drift. Another model with ω_1 =1.96 and L/h =1.67 can still achieve the highest drift ratio capacities.

According to the design equation given in Eq. (5), for the same t_w and h_s, as L increases, the required minimum column moment of inertia decreases. This is per the limit value of 2.5 is adopted for ω_1 for both narrow and broad SPSWs in the provisions. Thus, for models with high L/h ratio design code yields columns with lower minimum I_c value. However, according to results of this study, L/h ratio is inversely correlated to good behavior when used together with flexible columns. So, it should be safer to adopt the limiting ω_1 value of 2.2 for steel plate shear walls with large bay width ($L/h \geq 1.67$). As the stress uniformity diminishes due to inadequate tension field development in high aspect ratio models, so columns should be stiffer to allow steel infill to develop a full tension field mechanism.

When the array with 292 models is evaluated considering the I_c/I_b ratio, for two failure groups with the highest average I_c/I_b ratio, the results indicate that both groups have failure at the top beam. Looking at the two groups with the lowest I_c/I_b ratio, the results show that the failures occur in the columns. According to the adequately designed SPSW's failure sequence, it is desirable that the hinging occurs first in the beams and then in the columns. In this case, this parameter can be chosen depending on the column flexibility factor. For instance, allowing a low I_c/I_b ratio (≤ 2.0) for models with a column flexibility parameter higher than 2.2 may result in sudden failure in the columns while the beams are not yet damaged (column out-of-plane buckling and flexural-torsional buckling). An upper bound limit for I_c/I_b ratio is not suggested in this study. The model behavior with high I_c/I_b values can be improved by increasing the top beam stiffness. When the I_c/I_b ratio is above 3.0, the top anchor beam stiffness must be high enough to resist column and infill plate-induced forces. For the top beam, the code-based beam stiffness assumptions ($\omega_1 \leq 2.50$) do not apply in most cases. As a general rule, for models with ω_1 value above 2.2, the minimum value of I_c/I_b should be 2.0.

In the design phase, axial load ratio is among the challenging parameters. Drift ratio capacity decreases as the axial load ratio increases as expected. For models with high axial load, it is necessary to use columns with low column flexibility to achieve higher drift levels. For example, the average axial load value of beam buckling and column shear buckling groups are 2.21, but the average drift ratio capacities of these groups are 0.04 and 0.18, respectively. Here, the column flexibility factor shows the most dominant effect. However, it is clear that other parameters also influence the occurrence of this difference.

For the V_p/V_t ratio, 0.75 turns out to be a decisive limit between failure modes. When this ratio is above 0.75, boundary elements tend to fail before the infill panel fully yields. Partially yielded plates do not comply with the SPSW design philosophy and cause undesirable system behavior by producing non-uniform stress fields. The contribution of boundary frame to the total shear force generally shows strong correlation with the column flexibility factor and the

steel infill aspect ratio. The increase in both parameters causes an increase in the share of steel infill plate in the load distribution. Although the most effective parameters in the ratio V_p/V_t are ω_i and L/h, other parameters also have reasonable effect on this ratio. The following equation is derived by regression analysis using all 292 analyses data for the prediction of V_p/V_t with design parameters. The R-squared value of the regression fit is 0.96.

$$\frac{V_p}{V_t} = 0.43\omega_i + 0.025\frac{I_c}{I_b} + 0.077\frac{b_f}{h_b} + 0.0056\frac{b_f}{2t_f} + 0.29\frac{L}{h} + 0.11\frac{P}{P_{cr}} - 0.773 \quad (7)$$

4. EVALUATION OF THE EFFECT OF PARAMETERS ON DESIGN EQUATIONS

For further examining the effects of the parameters on the global system behavior, an investigation on the V_p/V_t ratio is conducted. The V_p/V_t ratios from analyses are plotted with respect to column flexibility factor in Figure 14. The 292 models are divided into three groups considering the infill plate aspect ratios. Accordingly, the plate L/h ratio of the models in the first group is 0.67, the average L/h ratios of models in the second group are 1.11 and 1.33, and the L/h ratios of the last group are 1.67 and 2.00.

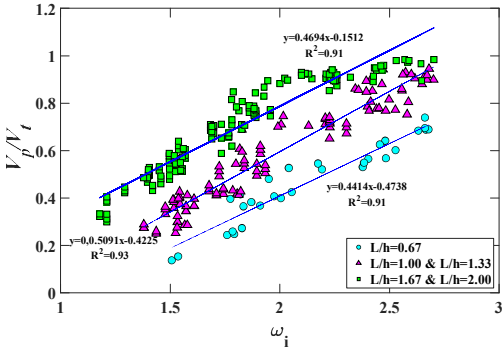

Figure 14- Relation of column flexibility factor ω_i and V_p/V_t.

The plot reveals that the V_p/V_t ratio at yield is directly proportional to the column flexibility parameter, and as the L/h ratio increases, the percentage of shear carried by plate V_p increases. The ω_i and L/h parameters are very effective in quantifying the shear percentage carried by plate and frame components of SPSW. All three datasets consist of models with different axial loads and different plate thickness. A general simplified form of Eq. (7) to predict the V_p/V_t ratio is calculated as;

$$\frac{V_p}{V_t} = 0.44 \times \omega_i + 0.31 \times \frac{L}{h} - 0.64 \quad (8)$$

The tension field inclination angles at all three stories are examined, but only the first story inclination angles are displayed here. The tension field inclination angle is determined based

on principal stress and principal strain directions. Figure 15(a) demonstrates the middle plate region on which tension field inclination angles are calculated. The width of the left and right column fields is *L/4*, and the middle plate field is *L/2*, where *L* is the infill plate length. Considering the inclined infill plate tension field mechanism, the principal strain and the principle stress angles with vertical direction are approximated to be tension field inclination angles. Both (principle stress and principle strain) angles are compared, and angles of the principal strains are found to be more stable and reliable. First story middle region tension field inclination angles that are obtained according to the principle strain angles are presented in Figure 15(b). According to the results, the permitted value of 40 degrees given by Seismic Provisions for Structural Steel Buildings [5] is found to be conservative, but an angle of 45 degrees is more realistic than 40 degrees. All models develop a tension field inclination angle between 42° and 47°. It is observed that the difference between the angle obtained from code-equation and FE analysis can rise to 14°. An inclination angle correction factor β for the code formula in Eq. (1) is proposed using the parameters; L, h, I_c, I_b, and ω_i. The right-hand-side of the tension field inclination angle equation is rearranged as;

$$\tan^4 \alpha = \beta \cdot \frac{1+\dfrac{t_w L}{2A_c}}{1+t_w h\left[\dfrac{1}{A_b}+\dfrac{h^3}{360 I_c L}\right]} \tag{9}$$

The correction factor, β, is derived by regression analysis as;

$$\beta = 2.5575 - 0.573\frac{L}{h} - 0.526\omega_i + 0.0504\frac{I_c}{I_b} \tag{10}$$

Comparison of inclination angles predicted by both uncorrected and the correction factor applied code formula in Eq. (9) with the values calculated from finite element analyses are plotted in Figure 15(c). As seen, the proposed inclination angle correction factor β significantly improves the prediction capacity of Eq. (9).

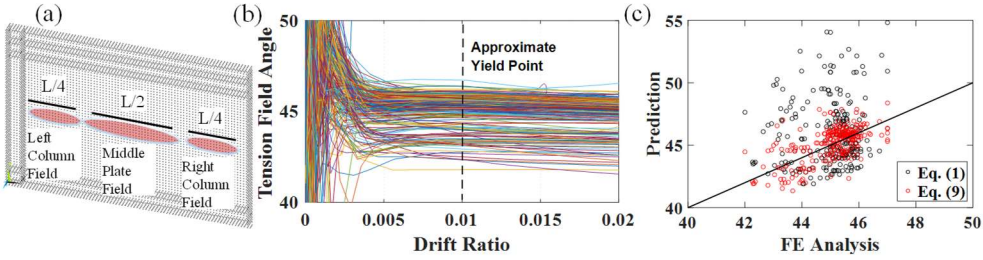

Figure 15 - (a) Regions on steel plate considered for the calculation of tension field angle, (b) Variation of tension field angle with top drift ratio, and (c) Comparison of predictions of tension field angle equations with and without correction factor and analyses results

As mentioned earlier, although provisions [5] incorporate equations such as Eq.(6) for the selection of horizontal boundary elements based on moments of inertia about an axis taken perpendicular to the plane of the web, a constant web plate thicknesses for all stories prevents us from using it. To better explore the effect of the horizontal boundary element stiffness on the behavior of SPSWs, I_b is introduced in proportion to I_c. All the analysis models are classified according to the I_c/I_b ratios. The I_c/I_b ranges of the groups are equal to 1, 1.8 to 2.2, 2.5 to 3.5 and greater than 3.5. For each group, the total shear force capacities from Eq. (3) and the analyses are compared in Figure 16(a). As seen in Figure 15, except for the I_c/I_b=1, the shear capacities calculated by Eq. (3) and finite element analyses agree well. When the moment frame shear force examined separately from the total shear, it is found that for I_c/I_b=1, $4M_p/h$ term calculating the frame contribution to total shear in Eq. (3) overestimates the shear strength of the frame approximately 2.2 times larger than FE analyses as displayed in Figure 16(b).

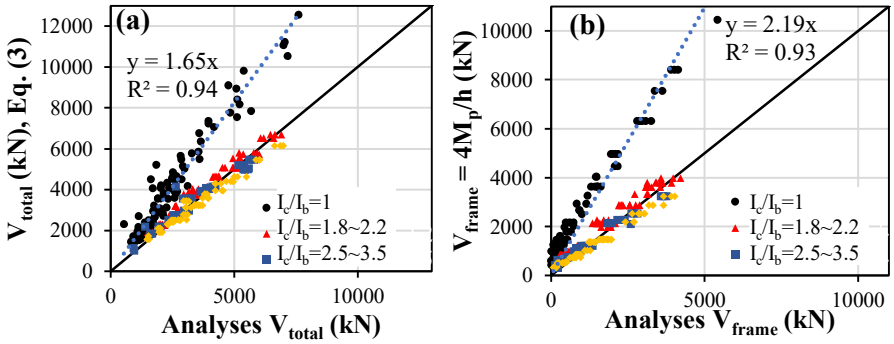

Figure 16 - Comparison of (a) the total SPSW shear force from FE analyses and prediction by Eq. (3), (b) the frame shear force from analyses and prediction by $4M_p/h$

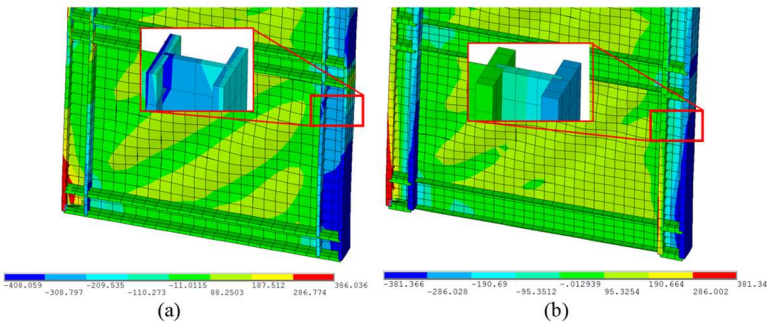

Figure 17 - Vertical stress distributions of a representative model with the ratio of (a) I_c/I_b equal to 1 and (b) I_c/I_b greater than 1

As given in Eq. (3), the contribution of frame to the total shear strength of SPSW is estimated as $4M_p/h$ on the premise that the plastic hinge mechanism develops either at beam or column

ends. However, for the cases, which the equation overestimates the frame shear force, the column at the compression side of the SPSW is primarily under the effect of axial force and only a minor bending moment as indicated by the distribution of the vertical stress along the column section given in Figure 17(a). The increasing axial force and the plate-induced span loading causes in-span buckling of column and a hinge develops at around half height of the column. Due to this mechanism, the equilibrium of forces produces a small shear force on compression side columns. Therefore, the contribution of the VBEs to the total shear force decreases to a value, which is almost $2M_p/h$, primarily from the tension side column. Thus, if the ratio I_c/I_b is ≈1, the expression $4M_p/h$ given in Eq. (3) should be used as $2M_p/h$. Figure 17(b) presents the stress distribution on a model with I_c/I_b>1. Tension and compression stresses at opposite flanges combine to form the bending moment acting on the section.

5. CONCLUSIONS

In this study, a total of 292 three-story steel plate shear wall systems are analyzed by using finite element method. The inelastic behavior of steel plate shear wall systems under monotonic loading are investigated. Limitations of preliminary design equations are determined on the basis of failure pattern, drift capacity and shear force distribution among panel and frame components of SPSWs on the FE models. The following main conclusions are derived from the parametric investigation.

- Seven different failure patterns are classified by evaluating the finite element analyses results and the relation of design parameters with these failure modes are evaluated. The failures related to column local instabilities (such as flange buckling or web twisting) is characterized with low drift ratio capacity and inefficient shear force distribution among frame and plate components of SPSW (V_p/V_t>0.75). In general, this behavior is observed when ω_1>2.2, and as the aspect ratio of wall becomes larger drift capacity reduces significantly. For such flexible systems (ω_1>2.2 and L/h>1.5), I_c/I_b ratio should be greater than 2 for improving the performance of the SPSWs.
- A column flexibility factor of 2.2 is proposed as a limit value for satisfactory column performance, improved drift capacity and balanced strength distribution among frame and panel of SPSW. Below this value, L/h and I_c/I_b ratios play a key role on the failure mode of the SPSW. For ω_1 <2 and L/h and I_c/I_b ratios are higher than 1.5 and 3, respectively, models tend to experience a sudden failure due to top beam buckling without any softening behavior on the load-deformation curve. When L/h is smaller than 1.5 (narrow SPSW), but I_c/I_b ratio is still higher than 3, the top beam fails in shear mode. The best performance is obtained when ω_1<2.2, L/h <1.5 and I_c/I_b<2.5.
- When more compact beams (represented by small $b_f/2t_f$ ratio) are used with strong columns (low ω_1) drift capacity increases. First three failure modes with the highest drift capacity, have the lowest average beam $b_f/2t_f$ ratios.
- The axial load ratio is an important determining parameter in the formation of patterns. A structure without vertical load is far from reality and also leads to inadequate code-limit definitions as shown in this study. This parameter affects both the drift capacity of the structure and the stability of the column.

- The value of 0.75 for V_p/V_t ratio has emerged as a critical threshold value for the strength distribution among plate and frame. According to the results of this study, design of boundary frame according to twenty-five percent boundary frame resistance is found to be reasonable to obtain improved SPSW performance.
- Tension field inclination angle at yield varies between 42 degrees and 47 degrees for all 292 models. The 45 degree value is found to be an effective value to use for design purposes. A correction factor that increases the accuracy of predictions is introduced into traditional inclination angle formula.
- Infill plate-shear wall interaction is strongly dependent on the aspect ratio of the infill plate and column flexibility factor of the system. No strong correlations are found with regard to infill plate thickness and axial load. When the aspect ratio (L/h) is smaller, infill plate shear force ratio to total shear force is lower. Greater column flexibility factor increases the percentage of shear force resisted by infill plate. An equation is proposed to estimate the ratio of the plate strength over total strength.
- When the column moment of inertia and beam moment of inertia ratio (I_c/I_b) becomes close to 1, SPSW shear strength formula given by Eq. (3) overestimates the total shear strength of the system. This overestimation mainly originates from the plastic hinge mechanism, which is assumed to develop at beam or column ends. However, when beams and columns have equal stiffness columns are prone to develop in span hinges.

Symbols

A_b Beam cross sectional area

A_c Column cross sectional area

b_f Beam flange width

h_b Beam depth

h Infill plate height

I_b Beam moment of inertia about the strong axis

I_c Column moment of inertia about the strong axis

$I_{c,min}$ Minimum allowed moment of inertia of the column

L Infill plate length

M_{pb} Plastic moment capacity of the beam

M_{pc} Plastic moment capacity of the column

P_{cr} Nominal strength of the column

t_f Beam flange thickness

t_w Infill plate thickness

V_d Shear force demand

V_p Shear strength of the plate

V_s Design shear strength

V_t Total shear strengths of frame and infill plate

α Inclination angle

σ_u Ultimate strength of the material

σ_y Yield strength of the material

υ Poisson ratio

ω_i Column flexibility parameter

ω_L Flexibility parameter of top and bottom beams

References

[1] Dusak S, Yalçin C, Yelgin AN. Experimental investigation of using sandwich panels as infill plate in a steel plate shear wall. Teknik Dergi/Technical Journal of Turkish Chamber of Civil Engineers 2020;31:10413–39. https://doi.org/10.18400/TEKDERG.559036.

[2] Li CH, Tsai KC. Experimental responses of four 2-story narrow steel plate shear walls. Proceedings of 2008 Structural Congress, vol. 314, Vancouver, Canada, 2008. https://doi.org/10.1061/41016(314)101.

[3] Thorburn LJ, Montgomery CJ, Kulak GL. Analysis of steel plate shear walls. Edmonton, Canada, 1983.

[4] Timler PA, Kulak GL. Experimental Study of Steel Plate Shear Walls, 1983. https://doi.org/10.7939/R3C24QV49.

[5] AISC. Seismic Provisions for Structural Steel Buildings. ANSI/AISC 341 2016;16.

[6] Sabelli R, Bruneau M. Steel Plate Shear Walls (Steel Design Guide 20). American Institute of Steel Construction Inc, 2006.

[7] Berman J, Bruneau M. Plastic analysis and design of steel plate shear walls. Journal of Structural Engineering 129:1448–56, 2003.

[8] Wagner H. Flat sheet metal girder with very thin metal web: Part 1: General theories and assumptions. National Advisory Committee for Aeronautics, 1931.

[9] Kuhn P, Peterson JP, Levin LR. A summary of diagonal tension Part I: methods of analysis, 1952.

[10] Montgomery CJ, Medhekar M, Lubell AS, Prion HGL, Ventura CE, Rezai M. Unstiffened steel plate shear wall performance under cyclic loading. Journal of Structural Engineering 127:973–5, 2001. https://doi.org/10.1061/(ASCE)0733-9445(2001)127:8(973).

[11] CAN CSA. CSA-S16-09 limit states design of steel structures. Rexdale, Canadian Standard Association, 2009.

[12] AISC. Seismic Provisions for Structural Steel Buildings. Chicago, Illinois, 2005.

[13] Purba R, Bruneau M. Seismic performance of steel plate shear walls considering two different design philosophies of infill plates. II: Assessment of collapse potential (2014 b). Journal of Structural Engineering (United States) 141:1–12, 2015. https://doi.org/10.1061/(ASCE)ST.1943-541X.0001097.

[14] Berman JW. Seismic behavior of code designed steel plate shear walls. Engineering Structures 33:230–44, 2011. https://doi.org/10.1016/j.engstruct.2010.10.015.

[15] Verma A, Sahoo DR. Estimation of lateral force contribution of boundary elements in steel plate shear wall systems. Earthquake Engineering and Structural Dynamics 46:1081–98, 2017. https://doi.org/10.1002/eqe.2845.

[16] Hosseinzadeh SAA, Tehranizadeh M. Behavioral characteristics of code designed steel plate shear wall systems. Journal of Constructional Steel Research 99:72–84, 2014. https://doi.org/10.1016/j.jcsr.2014.04.004.

[17] Uang CM, Bruneau M. State-of-the-Art Review on Seismic Design of Steel Structures. Journal of Structural Engineering 144, 2018. https://doi.org/10.1061/(ASCE)ST.1943-541X.0001973.

[18] Qin Y, Lu JY, Huang LCX, Cao S. Flexural behavior of anchor horizontal boundary element in steel plate shear wall. International Journal of Steel Structures 17:1073–86, 2017. https://doi.org/10.1007/s13296-017-9017-6.

[19] Dastfan M, Driver RG. Flexural stiffness limits for frame members of steel plate shear wall systems. Proceeding, Annual Stability Conference, p. 321–34, 2008.

[20] Yu JG, Feng XT, Li B, Hao JP, Elamin A, Ge ML. Performance of steel plate shear walls with axially loaded vertical boundary elements. Thin-Walled Structures 125:152–63, 2018. https://doi.org/10.1016/j.tws.2018.01.021.

[21] Curkovic I, Skejic D, Dzeba I. Impact of column flexural stiffness on behaviour of steel plate shear walls. Ce/Papers 1:3023–32, 2017. https://doi.org/10.1002/cepa.354.

[22] Qu B, Guo X, Pollino M, Chi H. Effect of column stiffness on drift concentration in steel plate shear walls. Journal of Constructional Steel Research 83:105–16, 2013. https://doi.org/10.1016/j.jcsr.2013.01.004.

[23] Qu B, Bruneau M. Behavior of vertical boundary elements in steel plate shear walls. Engineering Journal 47:109–22, 2010.

[24] Sahoo DR, Sidhu BS, Kumar A. Behavior of unstiffened steel plate shear wall with simple beam-to-column connections and flexible boundary elements. International Journal of Steel Structures 15:75–87, 2015. https://doi.org/10.1007/s13296-015-3005-5.

[25] Gholipour M, Alinia MM. Behavior of multi-story code-designed steel plate shear wall structures regarding bay width. Journal of Constructional Steel Research 122:40–56, 2016. https://doi.org/10.1016/j.jcsr.2016.01.020.

[26] Matteis GDE, Formisano A, Mazzolani FM. Numerical analysis of slender steel shear panels for assessing design formulas. International Journal of Structural Stability and Dynamics 2007;7:273–94.

[27] Kazaz İ, Gülkan P. Süneklik düzeyi yüksek betonarme perdelerdeki hasar sınırları. Teknik Dergi/Technical Journal of Turkish Chamber of Civil Engineers 23:6113–40, 2012. https://doi.org/10.18400/td.74396.

[28] Lubell AS. Performance of unstiffened steel plate shear walls under cyclic quasi-static loading. University of British Columbia, 1997.

[29] Wang M, Shi Y, Xu J, Yang W, Li Y. Experimental and numerical study of unstiffened steel plate shear wall structures. Journal of Constructional Steel Research 112:373–86, 2015. https://doi.org/10.1016/j.jcsr.2015.05.002.

[30] Park H-G, Kwack J-H, Jeon S-W, Kim W-K, Choi I-R. Framed steel plate wall behavior under cyclic lateral loading. Journal of Structural Engineering 133:378–88, 2007. https://doi.org/10.1061/(asce)0733-9445(2007)133:3(378).

[31] Choi IR, Park HG. Ductility and energy dissipation capacity of shear-dominated steel plate walls. Journal of Structural Engineering 134:1495–507, 2008. https://doi.org/10.1061/(ASCE)0733-9445(2008)134:9(1495).

[32] ANSYS. ANSYS Mechanical APDL. © ANSYS, Inc 2011:www.ansys.com. https://doi.org/www.ansys.com.